Exosomes released by imatinib-resistant K562 cells contain specific membrane markers, IFITM3, CD146 and CD36 and increase the survival of imatinib-sensitive cells in the presence of imatinib

TEREZA HRDINOVA[1,2], ONDREJ TOMAN[1], JIRI DRESLER[3], JANA KLIMENTOVA[4], BARBORA SALOVSKA[5], PETR PAJER[3], OLDRICH BARTOS[6], VACLAVA POLIVKOVA[1], JANA LINHARTOVA[1], KATERINA MACHOVA POLAKOVA[1,7], HANA KABICKOVA[3], BARBORA BRODSKA[1], MATYAS KRIJT[1], JAN ZIVNY[7], DANIEL VYORAL[1,7] and JIRI PETRAK[1,8]

[1]Institute of Hematology and Blood Transfusion; [2]Department of Cell Biology, Faculty of Science, Charles University, 128 20 Prague 2; [3]Military Health Institute, Military Medical Agency, 160 01 Prague 6; [4]Faculty of Military Health Sciences, University of Defense in Brno, 500 02 Hradec Kralove; [5]Department of Genome Integrity, Institute of Molecular Genetics of The Czech Academy of Sciences, 142 20 Prague 4; [6]Department of Infectious Diseases, First Faculty of Medicine, Charles University and Military University Hospital Prague, 169 02 Prague 6; [7]Institute of Pathological Physiology, First Faculty of Medicine, Charles University, 128 20 Prague 2; [8]Biotechnology and Biomedicine Centre of The Academy of Sciences and Charles University (BIOCEV), First Faculty of Medicine, Charles University, 252 50 Vestec, Czech Republic

Received May 27, 2020; Accepted October 8, 2020

DOI: 10.3892/ijo.2020.5163

Abstract. Chronic myeloid leukemia (CML) is a malignant hematopoietic disorder distinguished by the presence of a BCR-ABL1 fused oncogene with constitutive kinase activity. Targeted CML therapy by specific tyrosine kinase inhibitors (TKIs) leads to a marked improvement in the survival of the patients and their quality of life. However, the development of resistance to TKIs remains a critical issue for a subset of patients. The most common cause of resistance are numerous point mutations in the BCR-ABL1 gene, followed by less common mutations and multiple mutation-independent mechanisms. Recently, exosomes, which are extracellular vesicles excreted from normal and tumor cells, have been associated with drug resistance and cancer progression. The aim of the present study was to characterize the exosomes released by imatinib-resistant K562 ($K562^{IR}$) cells. The $K562^{IR}$-derived exosomes were internalized by imatinib-sensitive K562 cells, which thereby increased their survival in the presence of 2 μM imatinib. The exosomal cargo was subsequently analyzed to identify resistance-associated markers using a deep label-free quantification proteomic analysis. There were >3,000 exosomal proteins identified of which, 35 were found to be differentially expressed. From this, a total of 3, namely the membrane proteins, interferon-induced transmembrane protein 3, CD146 and CD36, were markedly upregulated in the exosomes derived from the $K562^{IR}$ cells, and exhibited surface localization. The upregulation of these proteins was verified in the $K562^{IR}$ exosomes, and also in the $K562^{IR}$ cells. Using flow cytometric analysis, it was possible to further demonstrate the potential of CD146 as a cell surface marker associated with imatinib resistance in K562 cells. Taken together, these results suggested that exosomes and their respective candidate surface proteins could be potential diagnostic markers of TKI drug resistance in CML therapy.

Correspondence to: Mrs. Tereza Hrdinova, Institute of Hematology and Blood Transfusion, U Nemocnice 1, 128 20 Prague 2, Czech Republic
E-mail: tereza.kabickova@uhkt.cz

Dr Jiri Petrak, Biotechnology and Biomedicine Centre of The Academy of Sciences and Charles University (BIOVEC), First Faculty of Medicine, Charles University, Prumyslova 595, 252 50 Vestec, Czech Republic
E-mail: jpetr@lf1.cuni.cz

Abbreviations: CML, chronic myeloid leukemia; TKI, tyrosine kinase inhibitor; $K562^{IR}$, K562 imatinib-resistant; NGS, next-generation sequencing; ddPCR, droplet digital PCR; LFQ, label-free quantification; CFSE, carboxyfluorescein succinimidyl ester; FACS, fluorescent-activated cell sorting; TRPS, tunable-resistive pulse sensing; LC-MS/MS, liquid chromatography coupled with tandem mass spectrometry; AGC, automatic gain control; FDR, false discovery rate; MFI, mean fluorescence intensity

Key words: chronic myeloid leukemia, imatinib mesylate, drug resistance, proteomics, exosome, tyrosine kinase inhibitor, surface marker

Introduction

Chronic myeloid leukemia (CML) is a clonal myeloproliferative disease characterized by reciprocal translocation between

chromosomes 9 and 22, t(9;22). This translocation results in the formation of the Philadelphia (Ph) chromosome, which encodes the fusion BCR-ABL1 oncogene coding a constitutively active Bcr-Abl tyrosine kinase (1-3). The approval of the Bcr-Abl inhibitor, imatinib (Glivec®) for clinical use in 2001 led to a significant improvement in the survival rate and prognosis of patients with CML (4). However, 10-15% of patients develop resistance to imatinib or to new-generation Bcr-Abl inhibitors (5). The resistance to TKIs is primarily caused by point mutations in the Bcr-Abl kinase domain, although other mechanisms that have been proposed include amplification of the BCR-ABL1 gene, overexpression of the Bcr-Abl protein or the presence of additional chromosomal aberrations and mutations (5-8).

An increasing number of studies have suggested that drug resistance in cancer, including leukemia, could be mediated by exosomes (9,10). Exosomes are small (30-150 nm) extracellular membrane vesicles, that are released by cells into the microenvironment upon fusion of multivesicular bodies with the plasma membrane (11). Exosomes contain proteins, lipids, mRNA, microRNAs (miRNAs) and DNA (12,13) and may fuse with other cells (14). They affect numerous physiological and pathological processes, including cancer (15). Exosomes derived from CML cells have been shown to modulate leukemia progression either directly via stimulation of leukemia cells (16), or indirectly through stimulation of other cells involved in leukemia biology, such as macrophages, bone marrow stromal cells and endothelial cells (17-21). Notably, exosomes derived from imatinib-resistant CML cells have recently been shown to fuse with imatinib-sensitive CML cells, thereby increasing their survival in the presence of imatinib (22).

The aims of the present study were: i) To confirm the previously observed pro-survival effect of exosomes derived from imatinib-resistant K562 cells ($K562^{IR}$); ii) to characterize the protein cargo of the exosomes; and iii) to identify potential specific cell surface markers of imatinib resistance in CML cells.

Materials and methods

Materials. All chemicals, unless otherwise stated, were purchased from Merck KGaA.

Cell lines. The human K562 chronic myeloid leukemia cell line was purchased from the German Collection of Microorganisms and Cell Cultures, GmbH and cultured in RPMI medium (Thermo Fisher Scientific, Inc.) supplemented with 10% fetal bovine serum (FBS; Gibco; Thermo Fisher Scientific, Inc.), 100 U/ml penicillin G, 100 μg/ml streptomycin and 7.5% sodium bicarbonate at 37˚C in an humidified incubator with 5% CO_2. The $K562^{IR}$ cells were derived from original imatinib-sensitive K562 cells, that had been cultured in gradually increasing concentrations of imatinib in the culture medium (from 0.1 to 2 μM) for 9 months, as previously described (23). The concentration of imatinib was increased by 0.1 μM at each step and was maintained for 15-30 days, depending on the proportion of surviving cells. The resulting $K562^{IR}$ cell line was resistant to 2 μM imatinib.

Cell viability assay. The K562 and $K562^{IR}$ cell lines were cultured in the presence of different concentrations (0 to 2 μM) of imatinib for 3 days. Imatinib toxicity was determined by measuring cell viability using a Vybrant™ MTT cell proliferation assay kit (Thermo Fisher Scientific, Inc.), following the manufacturer's instructions. Proprietary solvent B containing SDS (from the kit) diluted with 0.01 M HCl was used to solubilize the purple formazan. Absorbance was detected at 570 nm using a microplate reader (Chameleon; Hidex Oy). Data was analyzed using MikroWin 2000 software, v4.0 (Mikrotek Laborsysteme GmbH).

Mutational analysis. The K562 and $K562^{IR}$ cell lines were analyzed using a next-generation sequencing (NGS) method, as previously described (24). Briefly, the amplicon library was prepared using a two-step selective amplification of cDNA, including the BCR-ABL1 kinase domain. At the first step, BCR-ABL1 cDNA was amplified, then primers, from the IRON II study (25), were used to prepare four 350 bp amplicons of the kinase domain. Sequencing was subsequently performed on a GS Junior 454 System, and the data was analyzed using the Amplicon Variant Analyzer software (both from Roche Diagnostics). The raw NGS data are freely available via NCBI Sequence Read Archive (https://www.ncbi.nlm.nih.gov/sra) under the project accession number, PRJNA664680, while the imatinib sensitive K562 and the imatinib resistant K562 cells have the accession numbers, SRX9210642 and SRX9210641, respectively.

BCR-ABL1 gene copy number analysis. The number of BCR-ABL1 gene copies was determined using the quantitative droplet digital PCR (ddPCR) method and a K562 specific assay based on the break-point sequence of the BCR-ABL1 gene (26). ddPCR was performed using a QX200 Droplet Digital PCR system and an Auto Droplet Generator (Bio-Rad Laboratories, Inc.) according to the manufacturer's instructions. The albumin gene was used as a control for the DNA reaction load. QuantaSoft™ v1.7.4.0917 software (Bio-Rad Laboratories, Inc.) was used for data analysis, and samples were analyzed in quadruplicate.

Measurement of BCR-ABL1 transcript levels. Total RNA was isolated from cells using TRIzol® (Thermo Fisher Scientific, Inc.) according to the manufacturer's instructions. cDNA was synthesized using 200 U M-MLV reverse transcriptase (Promega Corporation) and random hexamer primers (Jena Bioscience GmbH) according to the manufacturer's instructions, with incubation at 37˚C for 1 h and denaturation at 95˚C for 5 min. β-Glucuronidase (GUSB) was used as the control gene (27,28). The primers and probes for BCR-ABL1 and GUSB were designed, and the measurement of the expression levels were performed, according to the Europe Against Cancer protocol (29). The method has been standardized in the project of European Leukemia Net (30). The following primers and probes were used: GUSB forward, 5'-GAAAAT ATGTGGTTGGAGAGCTCATT-3, reverse 5-CCGAGT GAAGATCCCCTTTTTA-3 and fluorescein-containing probe, 5'-FAM-CCAGCACTCTCGTCGGTGACTGTT CA-BHQ1-3'; BCR-ABL1 forward, 5'-TCCGCTGACCAT CAATAAGGA-3', reverse 5'-CACTCAGACCCTGAGGCT CAA-3' fluorescein-containing probe, 5'-FAM-CCCTTC AGCGGCCAGTAGCATCTGA-BHQ1-3' (Integrated DNA

Technologies, Inc.). The following thermocycling conditions were used: Initial denaturation at 95˚C for 10 min and 45 cycles of 95˚C for 15 sec and 60˚C for 1 min. For RT-qPCR gene expression analysis, the ERM-AD623 reference material (Join Research Centre, Belgium) (31,32) was used to create the calibration curve for the determination of the number of copies of BCR-ABL1 and GUS gene.

Exosome isolation. The K562 and K562^{IR} cell lines were cultured for 5 days in RPMI medium with 10% exosome-depleted FBS. Exosomes were isolated from 200 ml cell culture media, as previously described (33). Briefly, conditioned medium was obtained as the supernatant from the centrifugation of live cells (300 x g for 10 min at 4˚C). Subsequently, dead cells were removed using a further round of centrifugation (2,000 x g for 10 min at 4˚C). The supernatant was filtered [using a Filtropur S syringe filter (0.22-μm membrane); Sarstedt AG & Co. KG] to remove larger vesicles and cell debris. The resultant suspension was then ultracentrifuged (100,000 x g for 70 min at 4˚C) using a Sorvall™ WX+ ultracentrifuge and a T647.5 fixed angle rotor (Thermo Fischer Scientific, Inc.). Exosome pellets were resuspended in PBS, and sedimented again (100,000 x g for 70 min at 4˚C).

Exosome visualization using transmission electron microscopy/negative staining. Isolated exosomes were resuspended in Trump's 4F:1G fixative, comprising 86 ml distilled water, 10 ml 40% formaldehyde (Merck KGaA), 4 ml 25% glutaraldehyde (Polysciences, Inc.), 1.16 g monosodium phosphate and 0.27 g sodium hydroxide (34), and adsorbed on Formvar/carbon coated grids conditioned with 1% Alcian blue in 1% acetic acid. The adsorbed particles were embedded in a layer of 2% phosphotungstic acid. Grids were viewed at 100 kV using a JEM 2000 CX microscope (JEOL, Ltd.) equipped with an Olympus MegaviewTM II digital camera (Olympus Corporation).

Particle size and concentration measurement using tunable-resistive pulse sensing (TRPS). An aliquot of exosomes resuspended in PBS was placed in the nanopore NP150 (qNano; Izon Science). All samples were measured at defined membrane stretch and with the same applied voltage at two different pressure levels (5 and 11 mbar). Calibration particles were measured directly after the sample measurement, and under identical conditions.

Exosome preparation for tandem mass spectrometry (MS/MS) analysis. A total of 5 independent isolations of exosomes, from both the K562 and K562^{IR} cell lines, were subjected to MS/MS analysis. The filter-aided sample preparation method was used, with some modifications (35). Exosomes in PBS were resuspended in 100 mM ammonium bicarbonate, transferred to spin columns (Amicon Ultra 0.5 ml 10 kDa MWCO centrifugal filters; Merck KGaA) and centrifuged at 26,000 x g for 20 min at 4˚C. The samples were then washed twice with 400 μl 100 mM ammonium bicarbonate and centrifuged again (26,000 x g for 20 min at 4˚C). RapiGest™ (0.1%; Waters Corporation) dissolved in 100 μl 50 mM Tris/HCl, (pH 7.5) was subsequently added to the samples in the spin columns, then the samples were incubated at 95˚C 10 min. After allowing the samples to cool down, 200 μl 0.1% RapiGest™ in 50 mM Tris/HCl, (pH 7.5) with 8 M guanidinium chloride was added, and the samples were subsequently incubated for 20 min at room temperature. The samples were then centrifuged at 18,000 x g for 25 min at 25˚C. Aliquots of the samples (10 μl) were taken, and the protein concentration was quantified using a QuantiPro™ BCA Assay kit (Sigma-Aldrich; Merck KGaA). Subsequently, the samples were reduced with 100 μl 100 mM (Tris)2-carboxyethyl phosphine hydrochloride for 30 min at 55˚C in a thermoshaker (Biosan, Ltd.) set at 600 rpm, alkylated with 100 μl 300 mM iodoacetamide at 37˚C for 30 min in the dark, then centrifuged at 12,000 x g for 35 min at 25˚C. Next, the samples were digested overnight at 37˚C using 2 μg sequencing-grade trypsin (Promega Corporation). The digested samples were then transferred into a new microtube for subsequent centrifugation (12,000 x g for 35 min at room temperature). Empore™ Solid Phase Extraction cartridges (C18; standard density, bed I.D., 4 mm) (3M Company) were used to desalt the peptide mixtures. Peptides were eluted in 60% acetonitrile (ACN)/0.1% trifluoroacetic acid (TFA), then dried in a SpeedVac. Prior to MS analysis, the samples were resuspended in 30 μl 2% ACN/0.1% TFA.

Liquid chromatography (LC) MS/MS (LC-MS/MS)

LC-MS/MS analysis. An UltiMate™ 3000 RSLCnano system controlled by Chromeleon software (Dionex; Thermo Fisher Scientific, Inc.) was used for LC separation. Aliquots (1 μl) of each sample (10X diluted) were loaded onto a PepMap100 C18, 3 μm, 100 Å, 0.075x20 mm trap column (Dionex; Thermo Fisher Scientific, Inc.) at 5 μl/min for 5 min. Peptides were then separated on a PepMap RSLC C18, 2 μm, 100 Å, 0.075x150 mm analytical column (Dionex; Thermo Fisher Scientific, Inc.) using a gradient formed by the mobile phase A [0.1% formic acid (FA)] and mobile phase B (80% ACN/0.1% FA), running from 4-34% in 68 min, and from 34-55% of mobile phase B in 21 min, at a flow rate of 0.3 μl/min at 40˚C. Eluted peptides were on-line electrosprayed into a Q-Exactive™ mass spectrometer using a Nanospray Flex ion source (Thermo Fisher Scientific, Inc.). Positive ion full-scan MS spectra (350-1,650 m/z) were acquired using a $1x10^6$ automatic gain control (AGC) target in the Orbitrap at 70,000 resolution. The top 12 precursors with charge state ≥2 and threshold intensity of $5x10^4$ counts were selected for higher-energy collisional dissociation fragmentation, with a dynamic exclusion window of 30 sec. The isolation window of 1.6 Da and normalized collision energy 27% was used. Each MS/MS spectrum was acquired at a resolution of 17,500, with a $1x10^5$ AGC target and a maximum 100 msec injection time.

Label-free quantification (LFQ): Raw data processing. The raw files were further analyzed using MaxQuant software, v1.5.3.30 (36) [with Andromeda as the search engine (37)] against the *Homo sapiens* subset of the SwissProt database (downloaded on 4th July 2019; 26,468 sequences). Only tryptic peptides, that were at least 7 amino acids in length, with up to two missed cleavages were considered. Mass tolerance was set to 4.5 ppm at the MS level, and 0.5 Da at the MS/MS level. The oxidation of methionine was set as a variable modification, and the carbamidomethylation of cysteine was set as a fixed modification. A false discovery rate (FDR) of 1% was used for peptide spectrum matches and protein identification using a

target decoy approach. Relative quantification was performed using the default parameters of the MaxLFQ algorithm (38), with the minimum ratio count set to 2.

LFQ: Data analysis. The 'proteinGroups.txt' MaxQuant output file was uploaded into Perseus (39) v1.5.2.6. Decoy hits, proteins only identified by site, and potential contaminants were removed. Protein groups quantified in at least four replicates out of five were considered for further $\log_2$ transformation of the LFQ intensities. Missing values were imputed from a normal distribution [Gaussian distribution width, 0.3 standard deviation (SD) and downshift 1.8 SD of the original data]. Data was normalized using the open source tool, Normalyzer (http://quantitativeproteomics.org/normalyzerde) and the variance stabilization normalization method (40). A Student's t-test (permutation based FDR 0.05, S0=0.1) was used for statistical analysis. Finally, proteins from this group with a fold change at least 1.5 were considered as being significantly different ($P<0.05$). Pearson's correlation test was performed to evaluate the inter-run reproducibility of individual LC-MS analyses. Proteins with known or expected cell-surface localization were selected using GenieScore, an algorithm for the prediction of surface localization (41). The Exocarta database (www.exocarta.org) was used to compare the proteins identified with those already found in exosomes.

Western blot analysis. The exosome pellets were lysed in 150 μl lysis buffer containing 140 mM sodium chloride, 10 mM HEPES, 0.15% Triton X100 and a protease inhibitor cocktail (1 tablet/10 ml; Roche Diagnostics), and subsequently incubated on ice for 20 min. The exosome samples were pooled and concentrated in an Amicon Ultra 0.5 ml 3 kDa MWCO centrifugal filter (Amicon Ultra; Merck KGaA) from 3 or 4 individual isolations. The protein concentration was determined using a Micro BCA™ protein assay kit (Pierce; Thermo Fisher Scientific, Inc.) according to the manufacturer's instructions, and protein samples were immediately frozen and stored at -80˚C.

The cell pellets were lysed in CelLytic™ M lysis buffer containing protease inhibitor cocktail (1 tablet/10 ml; Roche Diagnostics) on ice for 20 min. The cleared cell lysates were collected by centrifugation at 15,000 x g for 20 min at 4˚C, and the protein concentration was then determined using the Bradford method (Bio-Rad Laboratories, Inc.).

The lysate samples (30-60 μg) were mixed with Laemmli sample buffer (Bio-Rad Laboratories, Inc.) containing 2-mercaptoethanol and separated on 4-15% or 7.5% (in the case of Bcr-Abl separation) precast gels (Mini PROTEAN® TGX™; Bio-Rad Laboratories, Inc.). The separated proteins were transferred onto polyvinylidene fluoride membranes using the iBlot system, according to manufacturer's instructions (Thermo Fisher Scientific, Inc.). The membranes were blocked for 1 h in SuperBlock™ blocking buffer (Thermo Fisher Scientific, Inc.) and incubated overnight at 4˚C with primary antibodies diluted to 1:1,000 in PBST (PBS, 0.1% Tween-20). The following primary antibodies were used: Anti-c-Abl rabbit polyclonal antibody (cat. no. 2862S; Cell Signaling Technology, Inc.), anti-Bcr-Abl mouse monoclonal antibody (7C6) (cat. no. ab187831; Abcam), anti-GAPDH rabbit monoclonal antibody (cat. no. SAB5600208; Merck KGaA), anti-IFITM3 (cat. no. 59212; Cell Signaling Technology, Inc.), anti-CD146 mouse monoclonal antibody (cat. no. 563619; BD Biosciences), anti-CD36 rabbit monoclonal antibody (cat no. 14347S; Cell Signaling Technology, Inc.) and EXOAB antibody kit 1 (Systems Biosciences, LLC) containing rabbit polyclonal antibodies against CD63, CD81, anti-CD9 and HSP70. After extensive washing in PBST, the membranes were incubated with secondary horseradish peroxidase-conjugated anti-rabbit antibody (cat. no. 7074P2) or anti-mouse antibody (cat. no. 7076P2) (both at 1:20,000 and from Cell Signaling Technology, Inc.) for 90 min at room temperature. Protein bands were detected with an enhanced chemiluminescence detection reagent (Cytiva) using a G:BOX imager (Syngene Europe), and quantified using ImageJ software, v1.8.0 (National Institutes of Health).

Exosome fluorescent labeling and uptake monitoring. Fresh exosomes were washed and resuspended in PBS at room temperature. A 10 mM stock solution of carboxyfluorescein succinimidyl ester (CFSE) (Invitrogen; Thermo Fisher Scientific, Inc.) was diluted to a final concentration of 20 μM and added to the exosomes. The suspension was subsequently mixed and incubated for 25-30 min at room temperature in the dark. The labeling process was stopped by adding 4 ml of cold complete media, containing 10% FBS on ice for 5 min. CFSE-labeled exosomes were diluted in 60 ml PBS, collected by ultracentrifugation (100,000 x g for 70 min at 4˚C) and resuspended in 1.5 ml cell culture media with K562 cells (500,000 cells/ml). CFSE-positive cells were observed under a FluoView FV1000 confocal laser scanning microscope (Olympus Corporation) using an UPlanSAPO 60x NA1.35 oil immersion objective (magnification, x60). A 488 nm laser was used for CFSE excitation, and fluorescence emission was detected with a high sensitivity GaAsP detector at 500-600 nm. Fluorescent images were processed using the FluoView software|(FV10 ASW v3.1; Olympus Corporation).

Exosomes and cell co-cultivation. The K562 cells were co-cultured with either $K562^{IR}$-derived or K562-derived exosomes for 4 h, and then treated with 2 μM imatinib for 48 h. Cell viability was measured using a Vybrant® Cell Proliferation Assay kit (Thermo Fisher Scientific, Inc.); proprietary solvent B containing SDS was mixed with 0.01 M HCl and used to solubilize the purple formazan. The absorbance was measured at 570 nm using a microplate reader (Chameleon; Hidex Oy).

FACS analysis. The K562 and $K562^{IR}$ cells ($1.5x10^6$ cells) were washed in washing buffer (PBS supplemented with 0.1% BSA and 2 mM EDTA), centrifuged at 300 x g for 10 min at room temperature, then resuspended in washing buffer. Aliquots (50 μl) of the cell suspension (100,000 cells/tube) were transferred to FACS tubes and 1 μl anti-IFITM3 AF405 (cat. no. ITA8095; 1:50; G-Biosciences; Geno Technology, Inc.), 1 μl anti-CD146 (cat. no. 563619; 1:50; BD Biosciences) and 2 μl anti-Hu CD36 FITC (cat. no. 1F-451-T100; 1:25; EXBIO Praha, a.s.) were added. The samples were incubated in the dark for 30 min at room temperature, then washed again with 1 ml of washing buffer, prior to centrifugation (300 x g for 5 min at 25˚C). Washing buffer (250 μl) was added to the cell pellet, and the samples were analyzed using

flow cytometry, in triplicate, using BD FACSCanto™ II Cell Analyzer (BD Biosciences). The data was analyzed using BD FACSDiva software (v6.1.3; BD Biosciences). MFI was determined for the whole sample, and the fraction of positively stained cells (P2) was determined as the percentage of the parent population.

Statistical analysis. The data are expressed as the mean ± SD, from at least three replicates. Statistical analysis was performed using GraphPad Prism v8.0 software (GraphPad Software, Inc.). Relative resistance of K562 and K562^{IR} cells to imatinib was evaluated using an unpaired Student's t-test. For the investigation of cell survival following exosome exposure, one-way ANOVA with Tukey's post hoc test was used to determine the statistical significance. $P<0.05$ was considered to indicate a statistically significant difference.

Results

Development of imatinib resistant K562 cells. Imatinib-resistant K562^{IR} cells were derived from the originally imatinib-sensitive K562 cells [half-maximal inhibitory concentration (IC_{50}), 0.25-0.35 μM]. The K562^{IR} cells proliferated in imatinib concentrations exceeding 2 μM (Fig. 1).

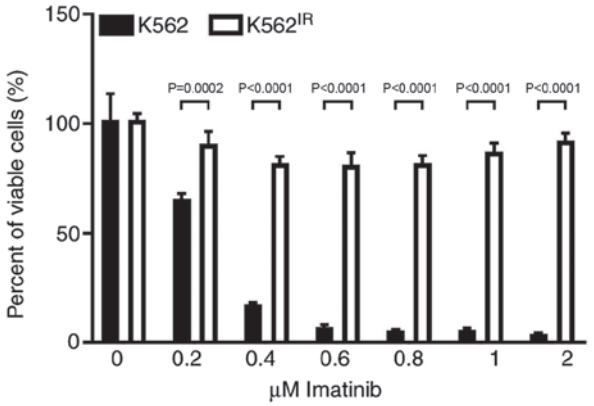

Figure 1. Relative viability of the K562 and K562^{IR} cells cultured in the presence of imatinib for 3 days. The viability was assessed using a MTT assay. Error bars indicate ± SD of three independent measurements. IR, imatinib-resistant.

Characterization of the K562^{IR} cells: Mutation analysis and BCR-ABL1 gene expression. A mutation in the kinase domain of BCR-ABL1 is the most common mechanism by which imatinib (and other TKIs) resistance develops in patients with CML (7). To investigate the mutational status of the BCR-ABL1 kinase domain in the K562^{IR} cells, NGS sequencing was performed; however, no mutations in the kinase domain, with variant allele frequency >1% were found. In patients with TKI resistance but without a kinase domain mutation, an amplification of the BCR-ABL1 gene is typically found (7). Therefore, ddPCR was used to identify the number of BCR-ABL1 gene copies, and it was revealed that the K562^{IR} cells harbored a 2-fold higher number of BCR-ABL1 gene copies compared with that in imatinib sensitive K562 cells (data not shown).

As the BCR-ABL1 gene amplification may result in overexpression of the BCR-ABL1 gene and increase the levels of the Bcr-Abl protein, the mRNA and protein expression levels were compared between the K562 and K562^{IR} cell lines. The results revealed increased expression levels of BCR-ABL1 mRNA (Fig. 2A) and of the Bcr-Abl protein (Fig. 2B).

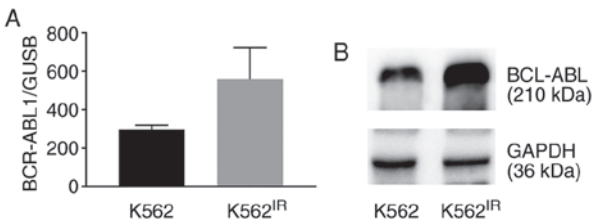

Figure 2. BCR-ABL1 mRNA and Bcr-Abl protein expression levels in the K562 and K562^{IR} cells. BCR-ABL1 (A) mRNA and (B) protein expression levels in the K562 and K562^{IR} cells were determined using reverse transcription-quantitative PCR and western blot analysis, respectively. IR, imatinib-resistant.

Exosome characterization. The exosomes were isolated from the K562 and K562^{IR} cell culture supernatants using ultracentrifugation. The exosome purity was verified using transmission electron microscopy, revealing round or cup-shaped vesicles, ranging between 50-150 nm in diameter (Fig. 3). The qNano/TRPS analysis of the exosomes confirmed comparable size distributions of the vesicles, with the highest peak occurring at 100-110 nm. The number of exosomes isolated from the cell media of the K562^{IR} cells ($1.67x10^{11}$ particles/ml) was ~2 times higher compared with that in the K562 cells ($8.14x10^{10}$ particles/ml) (Fig. S1).

To further confirm that the pelleted material represented exosomes, the presence of 'exosomal markers' i.e. proteins commonly found in exosomes (CD63, CD9, CD81, HSP70

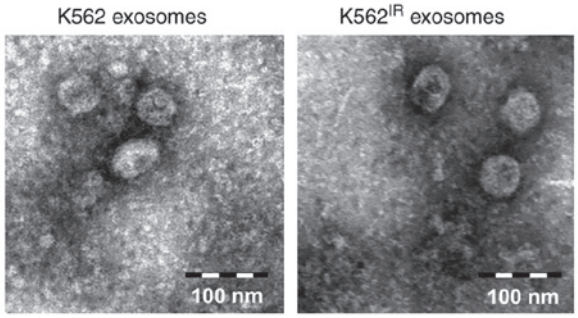

Figure 3. Exosomes from the K562 and K562^{IR} cells were visualized using transmission electron microscopy. Exosomes were defined as round or cup-shaped vesicles, at sizes between 50-150 nm. Scale bar, 100 nm. IR, imatinib-resistant.

and GAPDH) (42), was confirmed using western blot analysis (Fig. 4). As the CML landmark fusion protein, Bcr-Abl was overexpressed in the K562^{IR} cells, it was also possible to show the presence of the Bcr-Abl protein in the corresponding exosomes.

Uptake of K562^{IR}-derived exosomes by the K562 cells. K562-derived exosomes have been previously shown to be taken up by various cell types, such as bone marrow stromal cells, macrophages, endothelial cells and leukemic cells (16,17,19-21,43). Notably, exosomes derived from

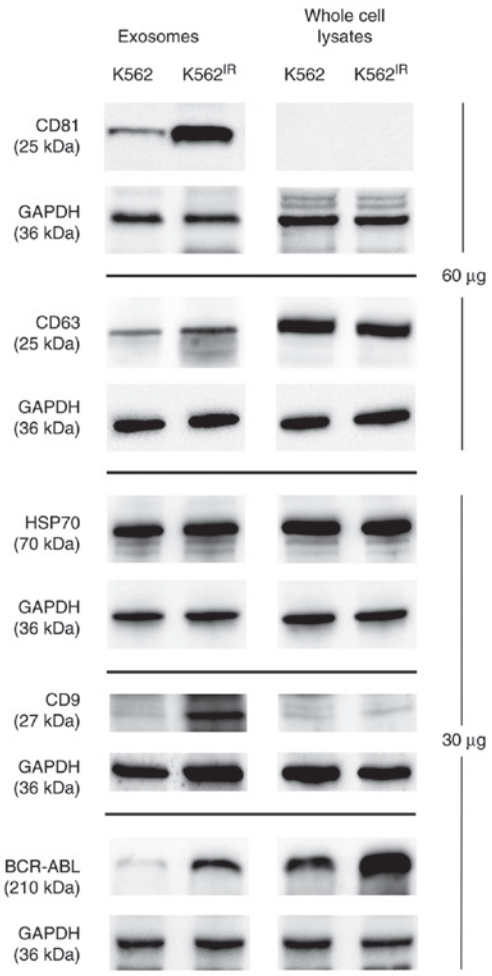

Figure 4. Presence of exosomal markers in the exosomes and cell lysates. Western blot analysis was used to detect the expression levels of known exosomal markers and the Bcr-Abl protein in exosomes isolated from the K562 and K562^{IR} cells, and in corresponding cells. For Bcr-Abl, CD9 and HSP70, 30 μg total protein was loaded for both exosomes and lysates, while 60 μg protein was loaded for CD63 and CD81. Exosomes and cell lysates that were to be probed by the same antibody were always loaded together on a single gel/membrane; the signals obtained are therefore comparable between exosomes and cell lysates. Irrelevant lanes have been cropped from the figure.

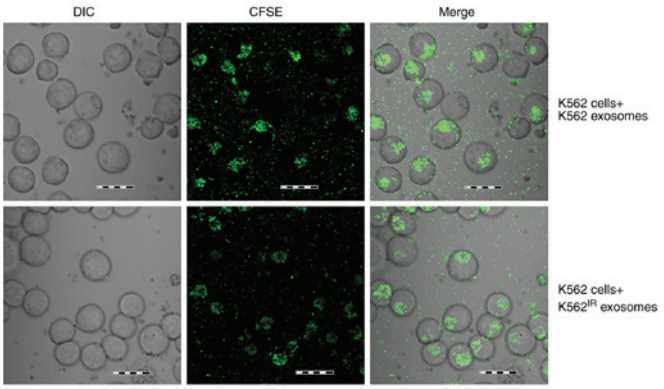

Figure 5. Internalization of the exosomes by the K562 cells visualized using confocal microscopy. The K562^{IR} exosomes loaded with CFSE (green) were internalized into the K562 cells and visualized in the cytoplasm after a 4-h incubation. Similarly, exosomes released from the imatinib-sensitive K562 cells were internalized into the K562 cells. Scale bar, 20 μm. CFSE, carboxyfluorescein succinimidyl ester; IR, imatinib-resistant.

imatinib-resistant CML cells have been recently shown to fuse with, and confer drug resistance traits to, imatinib-sensitive CML cells (22). In the present study, the fusion of K562^{IR}-derived exosomes (labelled with fluorescent CFSE) with K562 cells, and the fusion of K562-derived exosomes with K562 cells, was confirmed following a 4-h incubation (Fig. 5). CFSE-positive K562 cells were detected using confocal microscopy, as soon as 1 h after the addition of the labelled exosomes, with the maximum uptake occurring after 4 h, as determined in a pilot time-course experiment (data not shown).

Exosomes from K562^{IR} cells increase survival of K562 cells in the presence of imatinib. Min *et al* (22) demonstrated that exosomes released from imatinib-resistant K562 cells were able to transfer drug-resistant traits to imatinib-sensitive K562 cells. To confirm this observation, K562^{IR}- or K562-derived exosomes were isolated and incubated with K562 cells for 4 h, prior to the addition of imatinib (2 μM) for 2 days. As shown in Fig. 6, exosomes derived from the K562^{IR} cells significantly increased the survival rate of imatinib-sensitive K562 cells in the presence of imatinib, compared with the K562 cells incubated with exosomes derived from K562 cells, and also compared with the K562 cells treated with no exosomes. The control exosomes derived from the K562 cells; however, had no measurable effect on cell viability (Fig. 6).

Therefore, it could be hypothesized that the specific composition of the K562^{IR}-derived exosomes was responsible for the enhanced survival of the K562 cells. To characterize the unique protein content of the exosomes and to identify their specific (preferably surface) markers, a detailed proteomic analysis was subsequently performed.

LFQ proteomic analysis of the exosomes. Exosomes derived from the K562 and K562^{IR} cells were subjected to LFQ proteomic analysis. A total of 10 samples of the respective exosomes, obtained from five independent isolations of both the K562^{IR} and K562 cells, were analyzed using LC-MS/MS (Q-Exactive). With the FDR set to 0.01, between 1,072 and 1,751 exosomal proteins were identified in each sample; in total, 3,218 unique exosomal proteins were identified. Of those, 2,693 proteins were listed in the Exocarta database of exosomal proteomes (www.exocarta.org); therefore, the present study identified 525 novel exosomal proteins.

To determine the quantitative robustness of the label-free analysis, the quantitative similarity of all the LC-MS/MS runs was examined. Correlation analysis revealed good inter-sample reproducibility, with Pearson's correlation coefficients in the range of 0.723-0.971 (Fig. S2). The LFQ analysis provided semi-quantitative data for 1,241 proteins (Table SI).

Differentially abundant proteins. A total of 35 proteins with significantly different quantities were identified in the K562^{IR}-derived exosomes compared with the K562-derived exosomes (fold change >1.5) (Fig. 7 and Table I). Of these 35 proteins, 28 were found to be upregulated, while 7 were downregulated, in the K562^{IR} exosomes. The most upregulated proteins in the K562^{IR} exosomes included interferon-induced transmembrane protein 3 (IFITM3), desmoglein-2 (DSG2),

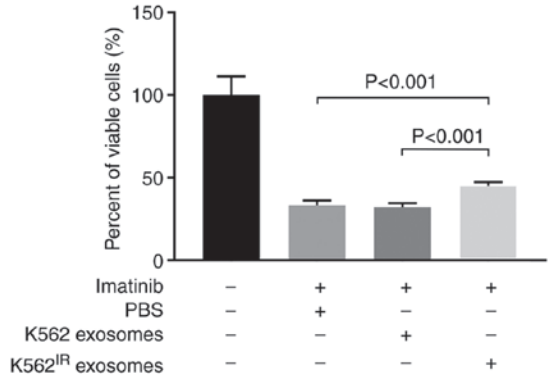

Figure 6. Incubation of the K562^{IR} exosomes with imatinib-sensitive K562 cells increases the cell viability of the K562 cells in the presence of 2 μM imatinib. One-way ANOVA with Tukey's post-hoc test was used. The mean values ± SD were calculated from three independent experiments. IR, imatinib-resistant.

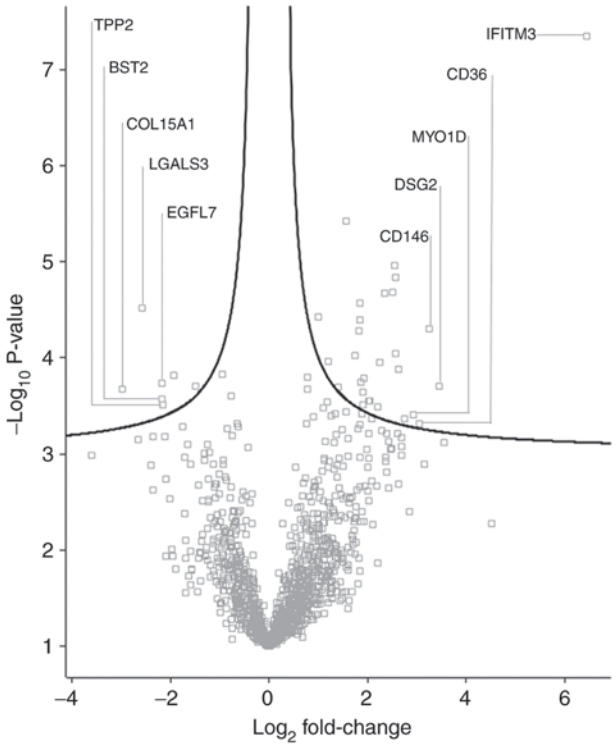

Figure 7. Differentially abundant exosomal proteins were identified using label-free quantification proteomic analysis of the K562 and K562^{IR} exosomes. Proteins with positive log2 fold change were upregulated in the K562^{IR} exosomes, while negative fold-change indicated proteins were down-regulated in the K562^{IR} exosomes. Only the proteins above the black line indicating statistical significance (false discovery rate <0.05, S0=0.1) were considered.

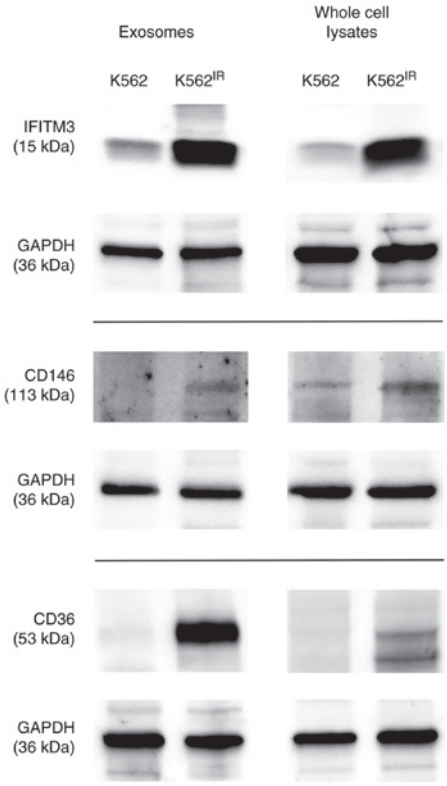

Figure 8. Confirmation of the differential abundance of IFITM3, CD146 and CD36 in the exosomes and cells using western blot analysis with specific antibodies. Protein samples (60 mg) were separated on precast 4-15% SDS PAGE gels. Irrelevant lanes have been cropped from the figure. IFITM3, interferon-induced transmembrane protein 3; IR, imatinib-resistant.

cell-surface glycoprotein MUC18 (CD146) and platelet glycoprotein 4 (CD36). Among the most downregulated were collagen α-1 (XV) chain, galectin-3-binding protein (LGALS3BP), laminin subunit β-1 (LAMB1), bone marrow stromal antigen 2 (BST2) and epidermal growth factor-like protein 7 (EGFL7).

The most highly upregulated proteins (at least 5-fold) were further investigated with special focus on proteins localized on the cell or exosomal membrane. Among the candidates selected by the LFQ proteomic analysis, three such proteins were identified using GenieScore, an algorithm for the prediction of surface localization (41): IFITM3, CD146 (MUC18) and CD36. The presence of these proteins was confirmed in the exosomes and also in the cells of their origin using western blot analysis with specific antibodies (Fig. 8).

The western blot data confirmed the upregulation of all three proteins in the K562^{IR}-derived exosomes, as well as in the 'source' K562^{IR} cells. Therefore, the upregulated surface membrane proteins could potentially serve, not only as exosomal markers, but also as cell-surface markers specific for a resistant population of the K562 cells.

IFITM3 and CD146 as specific surface markers of imatinib-resistant K562 cells. To determine the potential of the identified proteins as cell-surface markers of imatinib resistance, flow cytometric analysis of the K562 and K562^{IR} cells was performed using antibodies against IFITM3, CD146 and CD36. Live cells were used to determine the cell-surface expression of the putative markers.

Flow cytometry revealed markedly increased surface expression levels of IFITM3 and CD146, and to a lesser extent also of CD36, in K562^{IR} cells compared with the K562 cells (Fig. 9). CD146 was detected in 96.2% of the K562^{IR} cells compared with 0.7% of the K562 cells, while IFITM3 was detected in 51.6% of the K562^{IR} cells compared with 4% of the K562 cells. Anti-CD36 antibody stained 10.5% of the

Table I. Differentially abundant proteins in the $K562^{IR}$-derived exosomes, as compared with that in the K562-derived exosomes.

A, Upregulated protein in $K562^{IR}$ exosomes

Protein names	Protein IDs	Gene names	Fold change	Unique peptides	MS/MS	Permutation-based FDR
Interferon-induced transmembrane protein 3	Q01628	IFITM3	87.5	1	24	<0.001
Desmoglein-2	Q14126	DSG2	10.9	10	33	0.002
Cell surface glycoprotein MUC18	P43121	MCAM	9.6	11	28	<0.001
Platelet glycoprotein 4	P16671	CD36	8.4	7	18	0.005
Unconventional myosin-Id	O94832	MYO1D	7.6	21	41	0.004
CD2-associated protein	Q9Y5K6	CD2AP	6.7	29	105	0.004
Multivesicular body subunit 12A	Q96EY5	MVB12A	6.2	2	19	0.001
Golgi integral membrane protein 4	O00461	GOLIM4	6.0	18	37	<0.001
Protein TFG	Q92734	TFG	5.9	3	9	<0.001
Melanoma-associated antigen 4	P43358	MAGEA4	5.8	9	20	<0.001
Spastin	Q9UBP0	SPAST	5.7	9	19	<0.001
Melanotransferrin	P08582	MFI2	5.1	10	19	<0.001
Charged multivesicular body protein 4a	Q9BY43	CHMP4A	4.8	9	35	0.001
Tetraspanin-18	Q96SJ8	TSPAN18	4.6	3	13	0.003
Rab11 family-interacting protein 1	Q6WKZ4	RAB11FIP1	4.1	16	37	0.003
STAM-binding protein	O95630	STAMBP	4.1	9	16	0.003
Rac GTPase-activating protein 1	Q9H0H5	RACGAP1	3.8	10	18	0.002
Hepatocyte growth factor-regulated tyrosine kinase substrate	O14964	HGS	3.8	15	45	0.003
Protein tweety homolog 2	Q9BSA4	TTYH2	3.7	3	13	0.002
Toll-interacting protein	Q9H0E2	TOLLIP	3.7	4	24	0.002
Vacuolar protein sorting-associated protein 4A	Q9UN37	VPS4A	3.5	11	76	<0.001
Syntenin-1	O00560	SDCBP	3.6	22	207	<0.001
Hemoglobin subunit ε	P02100	HBE1	3.6	11	56	<0.001
Charged multivesicular body protein 4b	Q9H444	CHMP4B	3.3	15	86	<0.001
Crk-like protein	P46109	CRKL	3.0	12	56	<0.001
L-aminoadipate-semialdehyde dehydrogenase-phosphopantetheinyl transferase	Q9NRN7	AASDHPPT	2.6	6	10	0.002
Hemoglobin subunit ζ	P02008	HBZ	2.3	13	217	0.001
Heat shock protein 105 kDa	Q92598	HSPH1	2.0	19	79	<0.001

B, Downregulated proteins in $K562^{IR}$ exosomes

Protein names	Protein IDs	Gene names	Fold change	Unique peptides	MS/MS	Permutation-based FDR
DNA topoisomerase 2-β	Q02880	TOP2B	-2.8	7	23	0.002
Tyrosine-protein kinase receptor UFO	P30530	AXL	-3.8	7	21	0.002
Tripeptidyl-peptidase 2	P29144	TPP2	-4.4	57	211	0.003
Epidermal growth factor-like protein 7	Q9UHF1	EGFL7	-4.5	4	10	0.002
Bone marrow stromal antigen 2	Q10589	BST2	-4.5	6	17	0.003
Galectin-3-binding protein	Q08380	LGALS3BP	-5.9	6	17	0.001
Collagen α-1(XV) chain	P39059	COL15A1	-7.9	15	102	0.002

Positive fold change indicates upregulation, while negative fold changes indicates downregulation in $K562^{IR}$-derived exosomes. FDR, false discovery rate; MS, mass spectrometry.

$K562^{IR}$ compared with 3% of the K562 cells. The analysis demonstrated that CD146 expression, in particular, clearly distinguishes K562 from $K562^{IR}$ cells, and therefore it may be used as a reliable cell-surface marker of imatinib resistance in

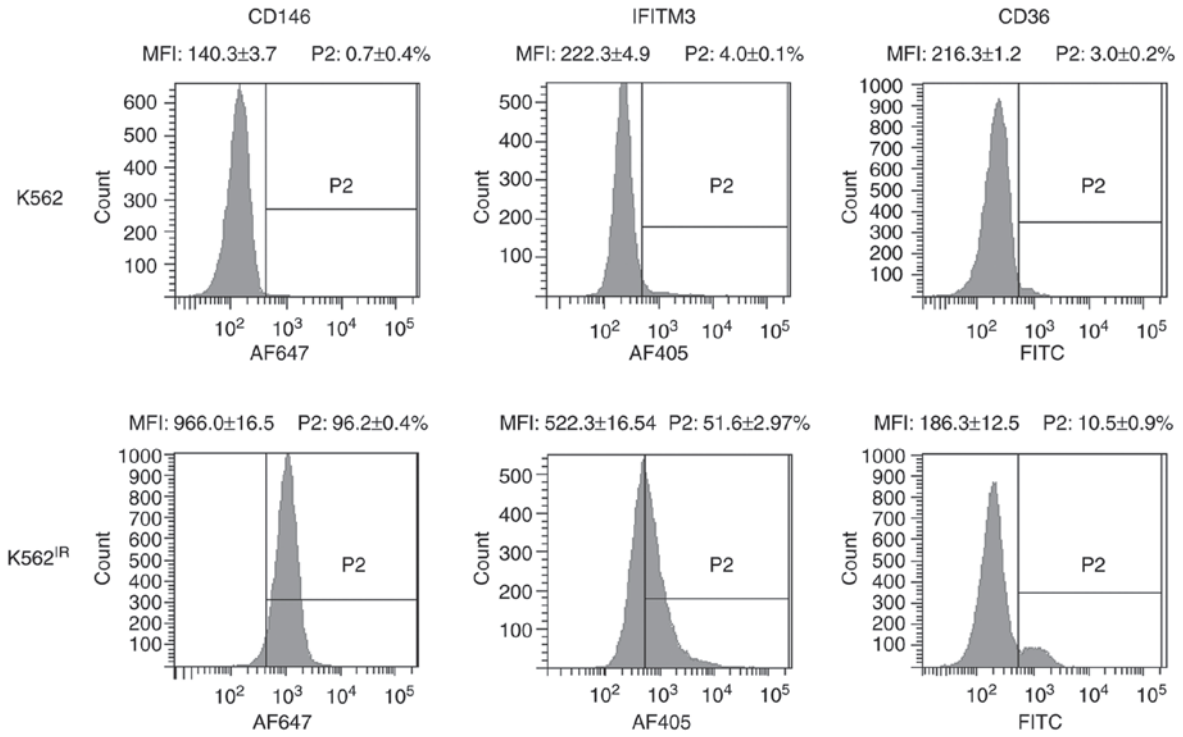

Figure 9. Surface-marker analysis of the K562 and K562^{IR} cells. Flow cytometry was used to confirm the increased expression of CD146, IFITM3 and CD36 on the surface of the K562^{IR} cells. The mean MFI and P2 values ± SD were calculated from three independent experiments. Representative graphs from repeated experiments are shown. IFITM3, interferon-induced transmembrane protein 3; MFI, mean fluorescence intensity; IR, imatinib-resistant.

these cells. In addition, promising results were also obtained with IFITM3.

Discussion

Incubation of isolated and carefully characterized K562^{IR}-derived exosomes with K562 cells, prior to exposure to imatinib, slightly, but significantly, increased the survival of the K562 cells in toxic doses of imatinib (2 μM). Thus, the results confirmed the observation Min *et al* (22) made in the same cell line, providing further evidence for the role of exosomes in the horizontal transfer of information among cancer cells, including pro-survival signals or a drug-resistance trait.

To what extent an exosome-mediated survival plays in the development of resistance to imatinib in patients with CML remains to be determined. A complex interaction between the resistant cells, exosomes and target cells can be hypothesized. The whole process can be spatially separated between the bone marrow and peripheral blood, and may include other than leukemic cells, for example, stromal cells in bone marrow, macrophages or endothelial cells (17,19-21). In addition, it could also be hypothesized that time may also play its role, namely with respect to potentially continuous production of exosomes *in vivo*. Furthermore, considering that several distinct molecular mechanisms of resistance to imatinib have been described (7,8), the role of exosome-mediated survival may differ among patients with CML. We propose that each individual mechanism of imatinib resistance may manifest with a different phenotype of the resistant cell population, affecting protein expression, cellular proliferation rate and other cellular properties, including exosomal content and the rate of exosome shedding. Mutations in the BCR-ABL1 kinase domain, which prevent interaction of imatinib with the Bcr-Abl protein, are the most common cause of resistance to imatinib in patients with CML (7). However, the K562^{IR} cells in the present study did not possess any mutations in the kinase domain; instead, BCR-ABL1 amplification resulted in overexpression at the mRNA and protein levels, which is another mechanism of resistance that has previously been described in specific patients with CML (6,44). This may suggest that the observations in the present study may be specific for the underlying mechanism of resistance in the model used, i.e. the overexpression of BCR-ABL1.

The role of exosomes in cancer progression and drug resistance establishes their potential as a source of biomarkers for monitoring the progression of the disease, the emergence of drug resistance, or the effects of a therapeutic intervention (9,15). A detailed characterization of the specific protein cargo of the exosomes and identification of resistance-associated markers on the surface of K562^{IR} exosomes and K562^{IR} cells was, therefore, performed. The LFQ proteome analysis identified over 3,000 exosomal proteins and provided relative quantitation for 1,241 of them. These datasets represent, to the best of our knowledge, the largest set of exosomal proteins derived from leukemic cells. Among the proteins with significantly different abundance in the K562^{IR} exosomes, the focus was directed to molecules known (or expected) to be localized on the surface of the cells and exosomes. Surface localization ensures proteins are easily accessible as markers or drug targets. A total of 3 significantly upregulated (i.e., >7-fold according the LFQ data) membrane proteins with predicted surface localization were identified in the K562^{IR} exosomes:

IFITM3, CD146 and CD36. Notably, all three putative marker proteins have been previously associated with cancer progression (45-57).

IFITM3 is a member of the interferon-induced transmembrane protein family (58), that is known for its antiviral activity, and has been associated with multiple viruses, including Middle East respiratory syndrome coronavirus (MERS-CoV) and severe acute respiratory syndrome coronavirus (SARS-CoV) (59). IFITM3 has also been found to be overexpressed in patients with AML and in human cell lines derived from gastric, lung, oral and breast tumors (45-49) and has been implicated in cancer progression (45,46), with either pro-proliferative and/or pro-migratory roles (47,48). High expression levels of IFITM3 protein have been associated with poor prognosis in acute myeloid leukemia (49).

CD146 is a transmembrane glycoprotein, that was first identified in malignant melanoma, where it contributed to metastasis (50). CD146 protein overexpression in various types of malignancies, such as melanoma, ovarian and breast cancer, and lung tumors, has been associated with tumor progression, angiogenesis and metastasis (51-53), and its expression has also been associated with drug resistance (54,55).

CD36 is a hematopoietic marker of a subpopulation of primitive (i.e., less differentiated) and blast crisis CML cells (56). Notably, these cell types are known to be less sensitive to imatinib (57). An increase in the protein expression level of CD36 could, therefore, potentially mark a sub-population of $K562^{IR}$ cells with a less differentiated myeloid phenotype.

Using specific antibodies, it was possible to confirm the increase of all three putative marker proteins in both the $K562^{IR}$ exosomes and the $K562^{IR}$ cells. Finally, to confirm the differential expression of IFITM3, CD146 and CD36 proteins on the surface of the $K562^{IR}$ cells and to validate their utility as potential marker of imatinib resistance, flow cytometric analysis of live K562 and $K562^{IR}$ cells was performed using specific antibodies. The results confirmed that CD146 could be a reliable positive marker of imatinib resistance in the K562 cells, which could be used to distinguish and separate populations of $K562^{IR}$ cells using flow cytometry. IFITM3 and CD36 displayed lower differences in expression levels, comparing between the K562 and $K562^{IR}$ cells, and, therefore, have a lower level of accuracy in terms of distinguishing between the resistant and the sensitive cell populations.

Due to their resistance-specific overexpression on the cell surface, CD146 and IFITM3 could be, at least theoretically, exploited as drug targets for molecular therapy in imatinib-resistant CML. In agreement with this, CD146 has been considered to be a promising therapeutic target in CD146-positive cancers, such as melanoma (60). The therapeutic potential of anti-CD146 antibodies for cancer therapy is already being evaluated (61). Similarly, IFITM3 inactivation (knockdown) studies (49,50) have also provided strong support for its future anti-cancer pharmacological potential.

The present study did not address the mechanism of exosome-mediated survival. However, several possible mechanisms may be proposed or envisioned. For example, we hypothesize that exosomes carrying the molecular target of the drug could shift the drug/target ratio in the recipient cells upon fusion. In the present study, BCR-ABL1 fusion gene amplification and overexpression were identified in the $K562^{IR}$ cells, which resulted in upregulation of the fusion kinase in the $K562^{IR}$ exosomes. The process of the causative kinase being delivered by $K562^{IR}$ exosomes to the recipient K562 cells may, thus, hypothetically shift the imatinib/Bcr-Abl ratio and increase the survival rate of the K562 cells.

Alternatively, and additionally, exosomes may transfer other pro-survival molecules or their precursors, namely proteins, RNAs or DNAs. In their original study, Min *et al* (22) identified miR-365 as a molecule partly responsible for the pro-survival effect of exosomes derived from imatinib-resistant K562 cells. However, the beneficial effect of miR-365 alone was lower compared with the administration of the whole exosomes (22), suggesting that other molecules are involved in the process. It is, therefore, possible to hypothesize that IFITM3 could be a potential pro-survival candidate molecule, as it regulates STAT3 phosphorylation (62) and signaling, leading to cell proliferation, angiogenesis and drug resistance (63). Similarly, CD146 could theoretically contribute to survival of the target cells, as it mediates chemoresistance in small-cell lung cancer and in breast cancer through the activation of AKT kinase (54,55). However, whether the CD146 and/or IFITM3 molecules contained within the 'resistant' exosomes are able to actually exert their signaling function in the recipient cells, thereby stimulating their survival in the presence of imatinib, remains to be determined.

It is well-known that the K562 cells represent a single cellular model of CML, which may differ significantly from the complex and heterogeneous situation in CML *in vivo*. Whether the markers identified in the $K562^{IR}$ model are also overexpressed in the leukemic cells of patients with imatinib resistant CML remains to be verified. Unfortunately, such a confirmatory study will be complicated by several factors. The therapy of patients with limited response to imatinib is promptly changed to a newer TKI (64), typically without bone marrow sampling. Therefore, leukemia cells from patients with CML that are truly resistant to imatinib are very rare. The future study would be required to include a large number of bone marrow samples obtained from patients with different degrees of response to imatinib. Secondly, the mechanisms of imatinib resistance may differ between patients, with and without mutations in the Bcr-Abl kinase domain, and the study must include both types of patients. Thirdly, the necessary isolation of Ph-positive leukemia cells from the complex bone marrow samples may severely limit the cellular material available for the verification of the candidate protein expression. Nevertheless, performing the verification study would be essential before proposing CD146 and IFITM3 as novel and clinically relevant markers of imatinib resistance, or potential drug targets for imatinib resistant CML.

Acknowledgements

Not applicable.

Funding

This study was supported by the Ministry of Education, Youth and Sports of the Czech Republic (grant nos. Progress Q26, SVV 260 521, UNCE/MED/016), the Ministry of

Health of the Czech Republic (grant nos. NC19-01-00083 and NC19-02-00130) and by the Project for Conceptual Development of Research Organizations (grant no. 00023736) of the Ministry of Health of the Czech Republic. The authors also acknowledge support from the projects CZ.1.05/2.1.00/19.0400 and CZ.1.05/1.1.00/02.0109 from the Research and Development for Innovations Operational Program co-financed by the European Regional Development Fund and the state budget of the Czech Republic. The LFQ MS work was supported by the Ministry of Interior, Czech Republic (grant no. VH20172020012) and by the Ministry of Defense of the Czech Republic through a long-term organization development plan (grant no. 907930101413). A grant was also provided from the Czech Academy of Sciences (grant no. L200521953).

Availability of data and materials

The datasets generated and analyzed during the current study have been deposited to the ProteomeXchange Consortium via the PRIDE (65) partner repository with the dataset identifier PXD019283.

Authors' contributions

TH, OT, DV and JP conceived the study and designed the experiments. TH, OT, JD, JK and PP were responsible for the LC-MS/MS data acquisition and interpretation. JL derived the resistant $K562^{IR}$ cells. VP performed BCR-ABL1 mutational, amplification and transcript analysis. KMP supervised the establishment of the resistant $K562^{IR}$, BCR-ABL1 NGS and ddPCR analyses and interpreted the data. HK performed the electron microscopy experiments. BB performed confocal microscopy. TH, BS and OB performed statistical analyses of the LFQ proteomic data. TH, MK and JZ performed the FACS analysis. JP and TK wrote the manuscript. All authors critically evaluated and approved the final version of the manuscript.

Ethics approval and consent to participate

Not applicable.

Patient consent for publication

Not applicable.

Competing interests

The authors declare that they have no competing interests.

References

1. Nowell PC and Hungerford DA: A minute chromosome in human chronic granulocytic leukemia. Science 132: 1497, 1960.
2. Rowley JD: Letter: A new consistent chromosomal abnormality in chronic myelogenous leukemia identified by quinacrine fluorescence and Giemsa staining. Nature 243: 290-293, 1973.
3. Heisterkamp N, Stephenson JR, Groffen J, Hansen PF, de Klein A, Bartram CR and Grosveld G: Localization of the c-abl oncogene adjacent to a translocation break point in chronic myelocytic leukaemia. Nature 306: 239-242, 1983.
4. Druker BJ, Talpaz M, Resta DJ, Peng B, Buchdunger E, Ford JM, Lydon NB, Kantarjian H, Capdeville R, Ohno-Jones S and Sawyers CL: Efficacy and safety of a specific inhibitor of the BCR-ABL tyrosine kinase in chronic myeloid leukemia. N Engl J Med 344: 1031-1037, 2001.
5. Lahaye T, Riehm B, Berger U, Paschka P, Müller MC, Kreil S, Merx K, Schwindel U, Schoch C, Hehlmann R and Hochhaus A: Response and resistance in 300 patients with BCR-ABL-positive leukemias treated with imatinib in a single center: A 4.5-year follow-up. Cancer 103: 1659-1669, 2005.
6. Gadzicki D, von Neuhoff N, Steinemann D, Just M, Büsche G, Kreipe H, Wilkens L and Schlegelberger B: BCR-ABL gene amplification and overexpression in a patient with chronic myeloid leukemia treated with imatinib. Cancer Genet Cytogenet 159: 164-167, 2005.
7. Gorre ME, Mohammed M, Ellwood K, Hsu N, Paquette R, Rao PN and Sawyers CL: Clinical resistance to STI-571 cancer therapy caused by BCR-ABL gene mutation or amplification. Science 293: 876-880, 2001.
8. Mahon FX, Deininger MW, Schultheis B, Chabrol J, Reiffers J, Goldman JM and Melo JV: Selection and characterization of BCR-ABL positive cell lines with differential sensitivity to the tyrosine kinase inhibitor STI571: Diverse mechanisms of resistance. Blood 96: 1070-1079, 2000.
9. Steinbichler TB, Dudas J, Skvortsov S, Ganswindt U, Riechelmann H and Skvortsova II: Therapy resistance mediated by exosomes. Mol Cancer 18: 58, 2019.
10. Nehrbas J, Butler JT, Chen DW and Kurre P: Extracellular vesicles and chemotherapy resistance in the AML microenvironment. Front Oncol 10: 90, 2020.
11. Johnstone RM, Adam M, Hammond JR, Orr L and Turbide C: Vesicle formation during reticulocyte maturation. Association of plasma membrane activities with released vesicles (exosomes). J Biol Chem 262: 9412-9420, 1987.
12. Valadi H, Ekstrom K, Bossios A, Sjostrand M, Lee JJ and Lotvall JO: Exosome-mediated transfer of mRNAs and microRNAs is a novel mechanism of genetic exchange between cells. Nat Cell Biol 9: 654-659, 2007.
13. Thakur BK, Zhang H, Becker A, Matei I, Huang Y, Costa-Silva B, Zheng Y, Hoshino A, Brazier H, Xiang J, *et al*: Double-stranded DNA in exosomes: A novel biomarker in cancer detection. Cell Res 24: 766-769, 2014.
14. Prada I and Meldolesi J: Binding and Fusion of Extracellular vesicles to the plasma membrane of their cell targets. Int J Mol Sci 17: 1296, 2016.
15. Maacha S, Bhat AA, Jimenez L, Raza A, Haris M, Uddin S and Grivel JC: Extracellular vesicles-mediated intercellular communication: Roles in the tumor microenvironment and anti-cancer drug resistance. Mol Cancer 18: 55, 2019.
16. Raimondo S, Saieva L, Corrado C, Fontana S, Flugy A, Rizzo A, De Leo G and Alessandro R: Chronic myeloid leukemia-derived exosomes promote tumor growth through an autocrine mechanism. Cell Commun Signal 13: 8, 2015.
17. Corrado C, Raimondo S, Saieva L, Flugy AM, De Leo G and Alessandro R: Exosome-mediated crosstalk between chronic myelogenous leukemia cells and human bone marrow stromal cells triggers an interleukin 8-dependent survival of leukemia cells. Cancer Lett 348: 71-76, 2014.
18. Cai J, Wu G, Tan X, Han Y, Chen C, Li C, Wang N, Zou X, Chen X, Zhou F, *et al*: Transferred BCR/ABL DNA from K562 extracellular vesicles causes chronic myeloid leukemia in immunodeficient mice. PLoS One 9: e105200, 2014.
19. Jafarzadeh N, Safari Z, Pornour M, Amirizadeh N, Forouzandeh Moghadam M and Sadeghizadeh M: Alteration of cellular and immune-related properties of bone marrow mesenchymal stem cells and macrophages by K562 chronic myeloid leukemia cell derived exosomes. J Cell Physiol 234: 3697-3710, 2019.
20. Taverna S, Flugy A, Saieva L, Kohn EC, Santoro A, Meraviglia S, De Leo G and Alessandro R: Role of exosomes released by chronic myelogenous leukemia cells in angiogenesis. Int J cancer 130: 2033-2043, 2012.
21. Mineo M, Garfield SH, Taverna S, Flugy A, De Leo G, Alessandro R and Kohn EC: Exosomes released by K562 chronic myeloid leukemia cells promote angiogenesis in a Src-dependent fashion. Angiogenesis 15: 33-45, 2012.
22. Min QH, Wang XZ, Zhang J, Chen QG, Li SQ, Liu XQ, Li J, Liu J, Yang WM, Jiang YH, *et al*: Exosomes derived from imatinib-resistant chronic myeloid leukemia cells mediate a horizontal transfer of drug-resistant trait by delivering miR365. Exp Cell Res 362: 386-393, 2018.

23. Toman O, Kabickova T, Vit O, Fiser R, Polakova KM, Zach J, Linhartova J, Vyoral D and Petrak J: Proteomic analysis of imatinib-resistant CML-T1 cells reveals calcium homeostasis as a potential therapeutic target. Oncol Rep 36: 1258-1268, 2016.
24. Machova Polakova K, Kulvait V, Benesova A, Linhartova J, Klamova H, Jaruskova M, de Benedittis C, Haferlach T, Baccarani M, Martinelli G, *et al*: Next-generation deep sequencing improves detection of BCR-ABL1 kinase domain mutations emerging under tyrosine kinase inhibitor treatment of chronic myeloid leukemia patients in chronic phase. J Cancer Res Clin Oncol 141: 887-899, 2015.
25. Kohlmann A, Grossmann V, Nadarajah N and Haferlach T: Next-generation sequencing-feasibility and practicality in haematology. Br J Haematol 160: 736-753, 2013.
26. Linhartova J, Hovorkova L, Soverini S, Benesova A, Jaruskova M, Klamova H, Zuna J and Machova Polakova K: Characterization of 46 patient-specific BCR-ABL1 fusions and detection of SNPs upstream and downstream the breakpoints in chronic myeloid leukemia using next generation sequencing. Mol Cancer 14: 89, 2015.
27. Moravcova J, Rulcova J, Polaková KM and Klamova H: Control genes in international standardization of real-time RT-PCR for BCR-ABL. Leuk Res 33: 582-584, 2009.
28. Rulcova J, Zmekova V, Zemanova Z, Klamova H and Moravcova J: The effect of total-ABL, GUS and B2M control genes on BCR-ABL monitoring by real-time RT-PCR. Leuk Res 31: 483-491, 2007.
29. Gabert J, Beillard E, van der Velden VH, Bi W, Grimwade D, Pallisgaard N, Barbany G, Cazzaniga G, Cayuela JM, Cavé H, *et al*: Standardization and quality control studies of 'real-time' quantitative reverse transcriptase polymerase chain reaction of fusion gene transcripts for residual disease detection in leukemia-a Europe Against Cancer program. Leukemia 17: 2318-2357, 2003.
30. Müller MC, Cross NCP, Erben P, Schenk P, Hanfstein B, Ernst T, Hehlmann R, Branford S, Saglio G and Hochhaus A: Harmonization of molecular monitoring of CML therapy in Europe. Leukemia 23:1957-1963, 2009.
31. Deprez L, Mazoua S, Corbisier P, Trapmann S, Schimmel H, White H, Cross N and Emons H: The certification of the copy number concentration of solutions of plasmid DNA containing a BCR-ABL b3a2 transcript fragment. Certified reference material: ERM-AD623a, ERM-AD623b, ERM-AD623c, ERM-AD623d, ERM-AD623e ERM-AD623f Luxembourg: Publications Office of the European Union; 2012. Report number EUR 25248; ISBN 978-92-79-23343-2, 2012.
32. White H, Deprez L, Corbisier P, Hall V, Lin F, Mazoua S, Trapmann S, Aggerholm A, Andrikovics H, Akiki S, *et al*: A certified plasmid reference material for the standardisation of BCR-ABL1 mRNA quantification by real-time quantitative PCR. Leukemia 29: 369-376, 2015.
33. Thery C, Amigorena S, Raposo G and Clayton A: Isolation and characterization of exosomes from cell culture supernatants and biological fluids. Curr Protoc Cell Biol Chapter 3: Unit 3.22, 2006.
34. McDowell EM and Trump BF: Histologic fixatives suitable for diagnostic light and electron microscopy. Arch Pathol Lab Med 100: 405-414, 1976.
35. Wisniewski JR, Zougman A and Mann M: Combination of FASP and StageTip-based fractionation allows in-depth analysis of the hippocampal membrane proteome. J Proteome Res 8: 5674-5678, 2009.
36. Cox J and Mann M: MaxQuant enables high peptide identification rates, individualized p.p.b.-range mass accuracies and proteome-wide protein quantification. Nat Biotechnol 26: 1367-1372, 2008.
37. Cox J, Neuhauser N, Michalski A, Scheltema RA, Olsen JV and Mann M: Andromeda: A peptide search engine integrated into the MaxQuant environment. J Proteome Res 10: 1794-1805, 2011.
38. Cox J, Hein MY, Luber CA, Paron I, Nagaraj N and Mann M: Accurate proteome-wide label-free quantification by delayed normalization and maximal peptide ratio extraction, termed MaxLFQ. Mol Cell Proteomics 13: 2513-2526, 2014.
39. Tyanova S, Temu T, Sinitcyn P, Carlson A, Hein MY, Geiger T, Mann M and Cox J: The Perseus computational platform for comprehensive analysis of (prote)omics data. Nat Methods 13: 731-740, 2016.
40. Chawade A, Alexandersson E and Levander F. Normalyzer: A tool for rapid evaluation of normalization methods for omics data sets. J Proteome Res 13: 3114-3120, 2014.
41. Waas M, Snarrenberg ST, Littrell J, Jones Lipinski RA, Hansen PA, Corbett JA and Gundry RL: SurfaceGenie: A web-based application for prioritizing cell-type specific marker candidates. Bioinformatics 36: 3447-3456, 2020.
42. Kowal J, Arras G, Colombo M, Jouve M, Morath JP, Primdal-Bengtson B, Dingli F, Loew D, Tkach M and Théry C: Proteomic comparison defines novel markers to characterize heterogeneous populations of extracellular vesicle subtypes. Proc Natl Acad Sci USA 113: E968-E977, 2016.
43. Tadokoro H, Umezu T, Ohyashiki K, Hirano T and Ohyashiki JH: Exosomes derived from hypoxic leukemia cells enhance tube formation in endothelial cells. J Biol Chem 288: 34343-34351, 2013.
44. Chandran RK, Geetha N, Sakthivel KM, Aswathy CG, Gopinath P, Raj TVA, Priya G, Nair JKKM and Sreedharan H: Genomic amplification of BCR-ABL1 fusion gene and its impact on the disease progression mechanism in patients with chronic myelogenous leukemia. Gene 686: 85-91, 2019.
45. Hu J, Wang S, Zhao Y, Guo Q, Zhang D, Chen J, Li J, Fei Q and Sun Y: Mechanism and biological significance of the overexpression of IFITM3 in gastric cancer. Oncol Rep 32: 2648-2656, 2014.
46. Zhang D, Wang H, He H, Niu H and Li Y: Interferon induced transmembrane protein 3 regulates the growth and invasion of human lung adenocarcinoma. Thorac Cancer 8: 337-343, 2017.
47. Yang M, Gao H, Chen P, Jia J and Wu S: Knockdown of interferon-induced transmembrane protein 3 expression suppresses breast cancer cell growth and colony formation and affects the cell cycle. Oncol Rep 30: 171-178, 2013.
48. Gan CP, Sam KK, Yee PS, Zainal NS, Lee BKB, Abdul Rahman ZA, Patel V, Tan AC, Zain RB and Cheong SC: IFITM3 knockdown reduces the expression of CCND1 and CDK4 and suppresses the growth of oral squamous cell carcinoma cells. Cell Oncol (Dordr) 42: 477-490, 2019.
49. Liu Y, Lu R, Cui W, Pang Y, Liu C, Cui L, Qian T, Quan L, Dai Y, Jiao Y, *et al*: High IFITM3 expression predicts adverse prognosis in acute myeloid leukemia. Cancer Gene Ther 27: 38-44, 2019.
50. Lehmann JM, Riethmuller G and Johnson JP: MUC18, a marker of tumor progression in human melanoma, shows sequence similarity to the neural cell adhesion molecules of the immunoglobulin superfamily. Proc Natl Acad Sci USA 86: 9891-9895, 1989.
51. Lei X, Guan CW, Song Y and Wang H: The multifaceted role of CD146/MCAM in the promotion of melanoma progression. Cancer Cell Int 15: 3, 2015.
52. Wu GJ and Dickerson EB: Frequent and increased expression of human METCAM/MUC18 in cancer tissues and metastatic lesions is associated with the clinical progression of human ovarian carcinoma. Taiwan J Obstet Gynecol 53: 509-517, 2014.
53. Watson-Hurst K and Becker D: The role of N-cadherin, MCAM and beta3 integrin in melanoma progression, proliferation, migration and invasion. Cancer Biol Ther 5: 1375-1382, 2006.
54. Tripathi SC, Fahrmann JF, Celiktas M, Aguilar M, Marini KD, Jolly MK, Katayama H, Wang H, Murage EN, Dennison JB, *et al*: MCAM Mediates Chemoresistance in Small-Cell Lung Cancer via the PI3K/AKT/SOX2 signaling pathway. Cancer Res 77: 4414-4425, 2017.
55. Liang YK, Zeng D, Xiao YS, Wu Y, Ouyang YX, Chen M, Li YC, Lin HY, Wei XL, Zhang YQ, *et al*: MCAM/CD146 promotes tamoxifen resistance in breast cancer cells through induction of epithelial-mesenchymal transition, decreased ERα expression and AKT activation. Cancer Lett 386: 65-76, 2017.
56. Ye H, Adane B, Khan N, Sullivan T, Minhajuddin M, Gasparetto M, Stevens B, Pei S, Balys M, Ashton JM, *et al*: Leukemic stem cells evade chemotherapy by metabolic adaptation to an adipose tissue niche. Cell Stem Cell 19: 23-37, 2016.
57. Landberg N, von Palffy S, Askmyr M, Lilljebjörn H, Sandén C, Rissler M, Mustjoki S, Hjorth-Hansen H, Richter J, Ågerstam H, *et al*: CD36 defines primitive chronic myeloid leukemia cells less responsive to imatinib but vulnerable to antibody-based therapeutic targeting. Haematologica 103: 447-455, 2018.
58. Bailey CC, Zhong G, Huang IC and Farzan M: IFITM-Family Proteins: The Cell's First Line of Antiviral Defense. Annu Rev Virol 1: 261-283, 2014.
59. Wrensch F, Winkler M and Pöhlmann S: IFITM proteins inhibit entry driven by the MERS-coronavirus spike protein: Evidence for cholesterol-independent mechanisms. Viruses 6: 3683-3698, 2014.

60. Nollet M, Stalin J, Moyon A, Traboulsi W, Essaadi A, Robert S, Malissen N, Bachelier R, Daniel L, Foucault-Bertaud A, *et al*: A novel anti-CD146 antibody specifically targets cancer cells by internalizing the molecule. Oncotarget 8: 112283-112296, 2017.
61. Stalin J, Nollet M, Dignat-George F, Bardin N and Blot-Chabaud M: Therapeutic and Diagnostic Antibodies to CD146: Thirty Years of Research on Its Potential for Detection and Treatment of Tumors. Antibodies (Basel) 6: 17, 2017.
62. Wang H, Tang F, Bian E, Zhang Y, Ji X, Yang Z and Zhao B: IFITM3/STAT3 axis promotes glioma cells invasion and is modulated by TGF-β. Mol Biol Rep 47: 433-441, 2020.
63. Johnston PA and Grandis JR: STAT3 signaling: Anticancer strategies and challenges. Mol Interv 11: 18-26, 2011.
64. Hochhaus A, Baccarani M, Silver RT, Schiffer C, Apperley JF, Cervantes F, Clark RE, Cortes JE, Deininger MW, Guilhot F, *et al*: European LeukemiaNet 2020 recommendations for treating chronic myeloid leukemia. Leukemia 34: 966-984, 2020.
65. Perez-Riverol Y, Csordas A, Bai J, Bernal-Llinares M, Hewapathirana S, Kundu DJ, Inuganti A, Griss J, Mayer G, Eisenacher M, *et al*: The PRIDE database and related tools and resources in 2019: Improving support for quantification data. Nucleic Acids Res 47: D442-D450, 2019.